

BRIEF DEFINITIVE REPORT

Hemolysis-associated phosphatidylserine exposure promotes polyclonal plasmablast differentiation

Rahul Vijay^{1*}, Jenna J. Guthmiller^{2*}, Alexandria J. Sturtz¹, Sequoia Crooks³, Jordan T. Johnson³, Lei Li², Linda Yu-Ling Lan⁴, Rosemary L. Pope⁴, Yani Chen⁵, Kai J. Rogers¹, Nirmal Dutta¹, Jason E. Toombs⁷, Mary E. Wilson^{1,3,5,6}, Patrick C. Wilson^{2,4}, Wendy Maury^{1,3}, Rolf A. Brekken^{7,8}, and Noah S. Butler^{1,3}

Antimalarial antibody responses are essential for mediating the clearance of *Plasmodium* parasite-infected RBCs from infected hosts. However, the rapid appearance of large numbers of plasmablasts in *Plasmodium*-infected hosts can suppress the development and function of durable humoral immunity. Here, we identify that the formation of plasmablast populations in *Plasmodium*-infected mice is mechanistically linked to both hemolysis-induced exposure of phosphatidylserine on damaged RBCs and inflammatory cues. We also show that virus and *Trypanosoma* infections known to trigger hemolytic anemia and high-grade inflammation also induce exuberant plasmablast responses. The induction of hemolysis or administration of RBC membrane ghosts increases plasmablast differentiation. The phosphatidylserine receptor Axl is critical for optimal plasmablast formation, and blocking phosphatidylserine limits plasmablast expansions and reduces *Plasmodium* parasite burden in vivo. Our findings support that strategies aimed at modulating polyclonal B cell activation and phosphatidylserine exposure may improve immune responses against *Plasmodium* parasites and potentially other infectious diseases that are associated with anemia.

Introduction

Malaria caused an estimated 409,000 deaths in 36 sub-Saharan African countries in 2019 (World Health Organization, 2020). Although severe anemia and cerebral malaria are significant causes of morbidity and mortality among infected children (Moxon et al., 2020; White, 2018), malaria-associated disease severity and *Plasmodium* pathogenesis can be limited by an effective humoral immune response. However, protective antibody responses are not efficiently induced by *Plasmodium* infections, and such humoral responses take years to develop among those living in malaria endemic areas (Tran et al., 2013), which leaves individuals susceptible to chronic and repeated bouts of infection.

Potent humoral immune responses elicited by vaccination and infection consist of temporally and spatially distinct B cell activation events that culminate in the formation of germinal center (GC)-derived memory B cells and long-lived plasma cells that are capable of producing class-switched high-affinity antibodies. The reasons for delayed and inefficient acquisition of antimalarial humoral immune responses are multifactorial

(reviewed in Ly and Hansen, 2019), but recent data support that GC responses induced by blood-stage *Plasmodium* infection are constrained by the rapid emergence of metabolically hyperactive populations of plasmablasts that numerically dominate the initial B cell response and suppress humoral immunity (Vijay et al., 2020). Using specific immunoassays, these studies further showed that only a small fraction (<1%) of the plasmablast population appeared parasite specific, consistent with blood-stage *Plasmodium* infection-associated polyclonal B cell activation.

Polyclonal B cell activation has been described as an immune evasion mechanism that multiple pathogens, including *Plasmodium*, have evolved to exploit in order to establish persistent infection, thereby increasing the likelihood for transmission. Initial work showed that the CIDR1 α subdomain of *Plasmodium falciparum* erythrocyte membrane protein-1 (PfEMP-1) could trigger B cell proliferation independent of B cell receptor (BCR) specificities (Donati et al., 2006; Donati et al., 2004; Simone et al., 2011). Additionally, controlled human malaria infection

¹Department of Microbiology and Immunology, The University of Iowa, Iowa City, IA; ²Department of Medicine, Section of Rheumatology, The University of Chicago, Chicago, IL; ³Interdisciplinary Graduate Program in Immunology, The University of Iowa, Iowa City, IA; ⁴Committee on Immunology, The University of Chicago, Chicago, IL; ⁵Department of Internal Medicine, The University of Iowa, Iowa City, IA; ⁶Department of Veterans Affairs Medical Center, Iowa City, IA; ⁷Hamon Center for Therapeutic Oncology Research, University of Texas Southwestern Medical Center, Dallas, TX; ⁸Departments of Surgery and Pharmacology, University of Texas Southwestern Medical Center, Dallas, TX.

*R. Vijay and J.J. Guthmiller contributed equally to this paper; Correspondence to Noah S. Butler: noah-butler@uiowa.edu.

© 2021 Vijay et al. This article is distributed under the terms of an Attribution-Noncommercial-Share Alike-No Mirror Sites license for the first six months after the publication date (see <http://www.rupress.org/terms/>). After six months it is available under a Creative Commons License (Attribution-Noncommercial-Share Alike 4.0 International license, as described at <https://creativecommons.org/licenses/by-nc-sa/4.0/>).

studies showed that the B cell growth and survival factor BAFF is potently induced during *P. falciparum* infection of malaria-naive individuals (Scholzen et al., 2014), which may additionally contribute to polyclonal B cell proliferation. Relevant to these sets of observations, *Plasmodium* blood-stage infection has been linked to the activation of self- and lipid-specific B cells (Rivera-Correa et al., 2017). The secretion of phosphatidylserine (PtS)-specific antibodies exacerbates anemia in experimental malaria models and is associated with severe malarial anemia in *P. falciparum*-infected individuals (Fernandez-Arias et al., 2016). As a composite, these reports suggest that the numerical over-representation of immunosuppressive and potentially self-reactive plasmablast populations triggered by *Plasmodium* blood-stage infection may be linked to polyclonal B cell activation events. However, the pathways and mechanisms that lead to the formation of rapid, high-magnitude plasmablast responses and whether the appearance of plasmablasts relates to distinct pathophysiologic features of malaria are not understood. Moreover, whether other infections associated with polyclonal B cell activation events also trigger high-magnitude plasmablast expansions has not been investigated.

Herein, we used comparative studies of microbial infections and combinations of transcriptomic analyses and biochemical and genetic approaches to explore these knowledge gaps. Our results reveal previously unrecognized stimuli that promote the differentiation and expansion of immunosuppressive plasmablast responses that include polyclonal B cell activation via IFN- γ and pathogen recognition receptor (PRR) signaling and hemolysis-associated exposure of PtS on RBC membranes. We further show exuberant plasmablast responses were also induced by virus and *Trypanosoma* infections that are associated with RBC damage and hemolysis and that blocking PtS in vivo during experimental malaria markedly reduced the formation of plasmablasts and improved parasite control. B cell-intrinsic expression of the PtS receptor Axl was also essential for optimal plasmablast expansion. Collectively, our data identify additional pathways that regulate nonspecific, polyclonal B cell activation and pathogen evasion of humoral immunity and reveal potential new targets to improve immune-mediated resistance to malaria and potentially other infectious diseases.

Results and discussion

Polyclonal B cell activation and CD138^{hi} plasmablast differentiation occur independently of antigen recognition by the BCR

10 d after the induction of experimental malaria in WT C57BL/6 mice, 50–70% of the entire activated (IgD^{neg}) splenic B cell pool is composed of CD138^{hi} immunosuppressive plasmablasts (Fig. 1 A and Fig. S1 A; Vijay et al., 2020). To investigate factors that promote the enormous expansions of malaria-associated plasmablasts, we first examined whether their appearance was linked to parasite burden. Across multiple time points, we observed a strong positive correlation between the proportion of CD138^{hi} plasmablasts among total B cells and parasite burden (Fig. 1 B), suggesting that pathogen-associated molecular patterns and/or antigen and BCR-associated activation events contribute to CD138^{hi} plasmablast expansion. However, RNA

sequencing analyses revealed transcriptional signatures that were consistent with blunted BCR-mediated activation in CD138^{hi} plasmablasts compared with CD138^{lo}IgD^{neg} activated B cells. Moreover, key pathways that include PI3K and BCR signaling showed lower activation scores (z score less than -1.5) in CD138^{hi} plasmablasts (Fig. 1 C and Table S1). Blunted BCR signaling was also evident by reduced phosphorylation of the tyrosine kinase Syk in CD138^{hi} plasmablasts compared with CD138^{lo}IgD^{neg} activated B cells (Fig. S1 B). CD138^{hi} plasmablasts also exhibited expected signatures of the unfolded protein response, yet substantially lower activation scores for genes associated with IFN- γ , TLR, and other PRR signaling pathways compared with activated B cells and naive B cells (Fig. 1 D, left and right, respectively; and Table S1).

These data raised the possibility that the differentiation of a proportion of *Plasmodium* infection-induced plasmablasts is either independent of BCR-antigen recognition and IFN- γ and PRR signaling or that plasmablasts are terminally differentiated and no longer express or engage these pathways, as do activated and naive B cells. To explore this hypothesis, we infected MD4 transgenic mice, in which the B cell repertoire is enriched for cells expressing a single BCR specific for hen egg lysozyme (HEL). Strikingly, numerically equivalent plasmablast expansions were observed (Fig. 1 E), and parasite control was equivalent through day 10 post-infection (p.i.; Fig. 1 F) in both *Plasmodium*-infected WT and MD4 mice. Expectedly, the sera of WT, but not MD4 mice, contained parasite-specific IgM and IgG antibody (Fig. 1 G, top). However, both genotypes harbored elevated HEL-specific antibody (Fig. 1 G, bottom), which is additionally consistent with polyclonal B cell activation following blood-stage *Plasmodium* infection. We also reacted sera from *Plasmodium*-infected WT mice against a panel of model antigens and bacterial components and identified robust IgM and IgG responses toward all antigens compared with naive mice (Fig. S1 C). Although parasite lysate-specific IgG titers remained elevated for 10 wk in *Plasmodium*-infected WT mice, anti-HEL and anti-LPS IgM and IgG responses markedly waned (Fig. S1 D), supporting that these off-target secreted antibody responses likely derive from short-lived, polyclonally activated plasmablasts. Consistent with nonspecific, polyclonal CD138^{hi} plasmablast activation and differentiation in *Plasmodium*-infected mice, single-cell transcriptomic analyses of the CD138^{hi} plasmablast BCR repertoire showed that it was as diverse as the naive B cell repertoire (Fig. 1 H and Fig. S1 E). Moreover, only two unique VH genes were selected within the plasmablast population (Fig. S1 F), suggesting that a very limited proportion of plasmablasts likely underwent BCR/antigen-dependent expansion. Together, these transcriptomic, genetic, and functional data support that a substantial proportion of the immunosuppressive CD138^{hi} plasmablast population expanded polyclonally during experimental malaria independently of canonical antigen recognition by BCR.

Optimal CD138^{hi} plasmablast expansion requires inflammatory cytokine and PRR signaling and is associated with hemolysis and RBC damage

Given that CD138^{hi} plasmablast expansion appeared to occur, in part, independently of antigen recognition by the BCR, we next

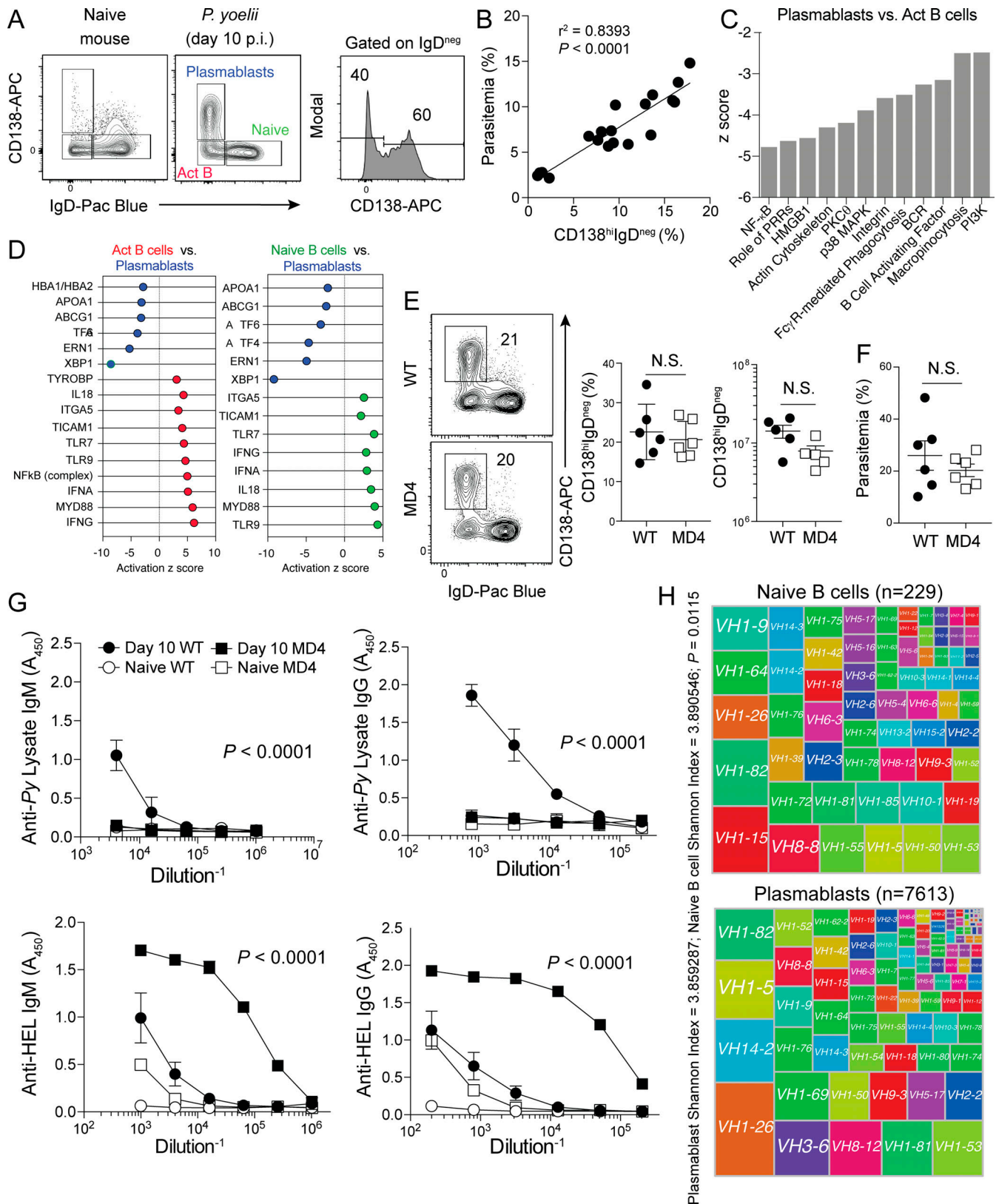


Figure 1. **Plasmablasts can expand independently of antigen-BCR interactions.** (A–D) WT mice were infected with 10^6 Py pRBCs. On days 4, 7, and 10 p.i., parasitemia, plasmablasts (CD138^{hi}IgD^{neg}), activated B cells (CD138^{lo}IgD^{neg}), and naive splenic B cell populations (CD138^{lo}IgD^{hi}) were quantified ($n = 19$). Using other WT mice ($n = 4$), the three B cell populations were sort-purified on day 10 p.i. and RNA sequenced for transcriptomic analysis. (A) Representative gating strategy showing plasmablasts, activated B (Act B) cells, and naive splenic B cells in either naive (left panel) or Py-infected mice (middle panel) on day 10 p.i. (B) Correlation graph showing frequency of plasmablasts (x axis) compared with frequency of infected RBCs (% parasitemia, y axis). (C and D) Canonical

pathways and upstream regulators of each phenotype were identified using Ingenuity Pathway Analysis software. **(C)** Pathways down-regulated (negative activation z score) in CD138^{hi} plasmablasts compared with activated B cells. **(D)** Left panel: Upstream regulators defining activated B cells (red) in comparison to CD138^{hi} plasmablasts (blue). Right panel: Upstream regulators defining naive B cells (green) in comparison to CD138^{hi} plasmablasts (blue). **(E)** WT and MD4 mice were infected with 10⁶ Py pRBCs. Representative plots, proportions, and total numbers of CD138^{hi}IgD^{neg} plasmablasts on day 10 p.i. $n = 5$ or 6 mice/group, mean \pm SEM, representative of two biologically independent experiments, analyzed by Mann-Whitney. **(F)** Parasitemia on day 10 p.i. **(G)** Anti-parasite lysate-specific IgM and IgG (top row) and anti-HEL-specific IgM and IgG (bottom row) antibody responses in sera from day 10 p.i. Data are mean \pm SEM, representative of six independent experiments, analyzed using two-way ANOVA. $n = 6$ mice/group, mean \pm SEM, representative of two biologically independent experiments, analyzed by Mann-Whitney. **(H)** Treemap diagrams of VH gene usage by naive B cells and plasmablasts recovered from infected mice on day 10 p.i. Shannon index indicates the diversity of the B cells within each population, and the number of cells within each population is listed above the diagrams. P value represents the median P value of 1,000 runs of Jack knife resampling of χ^2 tests.

tested whether other triggers of polyclonal B cell activation, including cytokine and PRR signaling, contribute to their expansion. Robust IFN- γ responses are key features of both clinical and experimental malaria (De Souza et al., 1997; King and Lamb, 2015). Although terminally differentiated plasmablasts exhibit reduced signatures of IFN- γ signaling (Fig. 1 D), the neutralization of IFN- γ in *Plasmodium*-infected MD4 mice reduced the number of CD138^{hi} plasmablasts by more than twofold (Fig. 2 A) and blunted anti-HEL-secreted IgM and IgG antibody titers by threefold to fourfold (Fig. S2 A). Chimeric mice in which *Ifn γ 1* deficiency was restricted to the B cell compartment (*B^{Ifn γ 1}-/-*) also exhibited threefold fewer CD138^{hi} plasmablasts compared with *B^{WT}* chimeric mice (Fig. 2 B). Moreover, the absence of TLR- and PRR-associated signaling adaptors MyD88 and TRIF reduced the differentiation and accumulation of CD138^{hi} plasmablasts by 30–40% (Fig. 2, C and D, respectively). The splenic B cell compartments in *MyD88*^{-/-} and *Ticam1*^{-/-} mice were 40–60% larger than those of WT mice, so the absolute number of plasmablasts was not different among these three groups (not shown). Together, these data support that the activity of polyclonal B cell activators, including IFN- γ and PRR signaling, and potentially other pathophysiological aspects of blood-stage malaria may act on precursor B cell populations to promote the induction and accumulation of terminally differentiated CD138^{hi} plasmablasts.

Because IFN- γ and two key PRR signaling pathways were required for optimal expansion of CD138^{hi} plasmablasts during experimental malaria, we hypothesized that high-magnitude CD138^{hi} plasmablast expansions would be observed in other systemic, pathological, and inflammatory immune insults. However, we observed minimal induction of splenic CD138^{hi} plasmablast responses in WT mice infected with either *Leishmania donovani* or *Leishmania infantum* (Fig. S2 B) or influenza A virus (Fig. S2 C) in type I IFN receptor-deficient mice infected with a recombinant vesicular stomatitis virus (VSV) or in WT mice infected with high-dose VSV (Fig. S2 D) or in septicemic WT mice subjected to cecal ligation and puncture (Fig. S2 E). By contrast, we observed marked CD138^{hi} plasmablast expansions in mice infected with either *Trypanosoma brucei* (*Tb*) or lymphocytic choriomeningitis virus strain Armstrong (LCMV-Arm; Fig. 2, E and F). These data led us to further hypothesize that in addition to IFN- γ and PRR signaling, other key pathological features of malaria, trypanosomiasis, and acute LCMV-Arm infection may also regulate the induction and expansion of CD138^{hi} plasmablasts. Indeed, polyclonal B cell activation, hemolysis, and anemia are features of both *Plasmodium* and *Tb* blood infections in

mice and humans (Ikede et al., 1977; Lamikanra et al., 2007; Stijlemans et al., 2018) and LCMV-Arm infection in mice (Stellrecht and Vella, 1992; von Herrath et al., 1999).

To test whether exacerbating hemolysis could augment the appearance and accumulation of CD138^{hi} plasmablasts, we induced acute hemolysis by administering phenylhydrazine hydrochloride (PHZ) to LCMV-infected mice. Administration of PHZ resulted in twofold to threefold increases in the frequency and number of CD138^{hi} plasmablasts in LCMV-infected mice but not naive mice (Fig. 2 F). PHZ-mediated hemolysis may stimulate CD138^{hi} plasmablast expansions via the release and recognition of either RBC cytoplasmic contents or damaged RBC membranes. To address whether membrane components were promoting plasmablast responses, we administered RBC membrane ghosts to LCMV-infected mice and found that RBC ghosts were sufficient to expand the number and proportion of CD138^{hi} plasmablasts by twofold (Fig. 2 G), which effectively phenocopied PHZ treatment. Together, these data suggest that the accumulation of infection- and inflammation-induced polyclonal CD138^{hi} plasmablast responses may be mechanistically linked to RBC damage and sensing of RBC membrane-associated factors.

PtS potentiates plasmablast differentiation and accumulation

Malaria induces RBC stress and associated translocation of PtS to the surface of both infected and noninfected RBCs (Fernandez-Arias et al., 2016), and PtS is a known antigenic target of self-phospholipid-specific, autoimmune antibody responses (Fernandez-Arias et al., 2016; Rivera-Correa et al., 2017; Rivera-Correa et al., 2019). Consistent with these reports, we found that substantial numbers of RBCs exposed PtS in our experimental *Plasmodium*-infected mice, as evidenced by Annexin V staining (Fig. 3 A), and appreciable levels of PtS-specific serum IgM and IgG antibodies were present on day 10 p.i. (Fig. 3 B), which coincides with the numerical peak of the immunosuppressive CD138^{hi} plasmablast response (Vijay et al., 2020). Sort-purified CD138^{hi} plasmablasts secreted detectable PtS-specific antibodies in both ELISA (Fig. 3 C) and ELISpot assays (Fig. 3 D), suggesting that a minor proportion of the polyclonal plasmablast response (~0.4%) includes cells expressing a BCR that targets self-lipid antigens.

Consistent with our *in vivo* data showing that IFN- γ and PRR signaling and hemolysis individually contribute to promoting plasmablast responses, we identified that naive B cells stimulated *ex vivo* with LPS and IFN- γ and in the presence of RBC ghosts up-regulated surface CD138 expression (Fig. 3 E) and

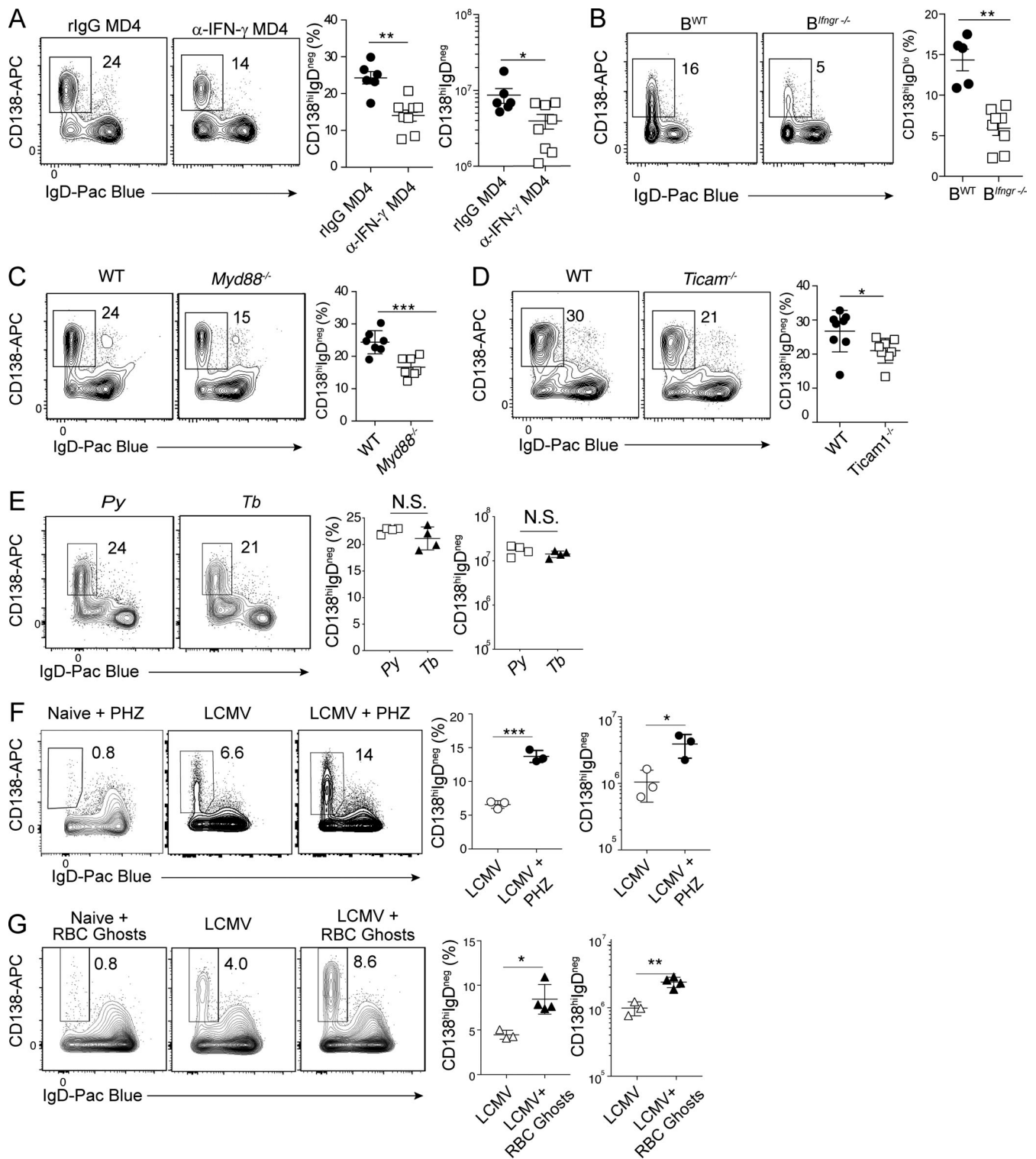


Figure 2. **Hemolysis augments plasmablast differentiation.** (A) MD4 mice were infected with 1×10^6 *Py* pRBCs and administered 500 μ g of α -IFN- γ (clone XMGI.2) or *rigG* on days 0, 3, 6, and 9 p.i. Representative plots, proportions, and total numbers of CD138^{hi}IgD^{neg} plasmablasts on day 10 p.i. $n = 6$ (*rigG*) and $n = 8$ (α -IFN- γ) mice/group; mean \pm SEM representative of six biologically independent experiments. (B) Representative flow plots and summary of WT or *Irfn1*^{-/-} B cells that differentiate into CD138^{hi}IgD^{neg} plasmablasts in individual B^{WT} and B^{*Irfn1*^{-/-}} competitive mixed bone marrow chimeric on day 10 p.i. $n = 9$ mice, data derived from two pooled experiments. $n = 9$ mice/group, mean \pm SEM, data derived from two pooled experiments. (C) Representative plots and proportions of CD138^{hi}IgD^{neg} plasmablasts on day 10 p.i. in $n = 7$ (WT) and $n = 7$ (*Myd88*^{-/-}) mice/group; mean \pm SEM, representative of two biologically independent experiments. (D) Representative plots and proportions of CD138^{hi}IgD^{neg} plasmablasts on day 10 p.i. in $n = 8$ (WT) and $n = 8$ (*Ticam1*^{-/-}) mice/group; mean \pm SEM, representative of two biologically independent experiments. (E) Representative plots and summary graphs showing splenic plasmablasts (CD138^{hi}IgD^{neg}) in *Py* and *Tb* infection on day 10 p.i. $n = 4$ mice/group; mean \pm SD, representative of two biologically independent experiments. (F) Representative plots and summary

graphs showing splenic plasmablasts (CD138^{hi}IgD^{neg}) on day 10 p.i. following LCMV infection with or without PHZ treatment. $n = 3$ mice/group; mean \pm SD, representative of two biologically independent experiments. (G) Representative plots and summary graphs showing splenic plasmablasts (CD138^{hi}IgD^{neg}) on day 10 p.i. following LCMV infection with or without RBC ghost administration. $n = 4$ mice/group; mean \pm SD, representative of two biologically independent experiments. Significance was calculated using Mann-Whitney (A, C–E, and G), paired t test (B), and Student's t test (F). *, $P < 0.05$; **, $P < 0.01$; ***, $P < 0.001$.

Prdm1 and *Xbp1* mRNA levels (Fig. 3 F), a gene signature that is characteristic of plasmablast differentiation (Iwakoshi et al., 2003a; Iwakoshi et al., 2003b; Shaffer et al., 2004). ELISA assays also confirmed that naive B cells stimulated with LPS, IFN- γ , and RBC ghosts secreted IgM (Fig. 3 G), supporting the notion that RBC membrane-associated factor(s) promote the induction and differentiation of CD138^{hi} plasmablasts.

Because both malaria (Fernandez-Arias et al., 2016) and PHZ treatment (Adams et al., 2002; White et al., 2013; Wu et al., 2014; Zhu et al., 2015) trigger PtS exposure in the outer leaflet of RBC membranes, we hypothesized that direct sensing of PtS exposed on damaged RBC membranes may promote the differentiation of CD138^{hi} plasmablasts, independently of BCR–PtS recognition. Indeed, we observed that a number of receptors documented to bind to PtS either directly (*Havcr1* encoding Tim1) or indirectly (*Mertk*, *Axl*, *Clqa*, *Clqb*, *Clqc*, *Scarbl*, and *Havcr2* encoding Tim2) were more highly expressed in naive or activated B cells compared with CD138^{hi} plasmablasts (Fig. 3 H). We also confirmed that splenic B cells recovered from both naive and *Plasmodium*-infected mice bound to PtS liposomes ex vivo, as detected by Annexin V labeling (Fig. S3 A), and that both resting (IgD^{hi}) and activated B cells (IgD^{neg}) from infected mice were equivalently labeled (Fig. S3 B). In further support of our hypothesis, ex vivo polyclonal activation of naive murine B cells in the presence of PtS, but not phosphatidylcholine (PtC), liposomes induced surface expression of CD138 (Fig. 3 I), up-regulation of *Prdm1* and *Xbp1* mRNA (Fig. 3 J), and IgM secretion (Fig. 3 K). Importantly, blocking either RBC ghosts or PtS liposomes with either Annexin V or the mouse chimeric monoclonal antibody (mch1N11) fully abrogated surface expression of CD138, induction of *Prdm1* and *Xbp1* mRNA, and IgM secretion (Fig. 3, E–G and I–K). We also found that substantial fractions of human peripheral B cells also acquired a plasmablast-like phenotype (CD27⁺CD38⁺) upon polyclonal stimulation and co-culture with either PtS liposomes or autologous RBC ghosts (Fig. 3 L). Collectively, these data support a model in which polyclonal B cell activation via IFN- γ and PRR signaling, coupled with either hemolysis- or RBC damage-associated PtS exposure and sensing, potentiates the differentiation and accumulation of plasmablasts.

Therapeutic blockade of PtS limits plasmablast responses and improves humoral immunity

PtS broadly functions as an immunosuppressive signal in the tumor microenvironment, and biologics that block PtS can boost immune activity and tumor control (Dayoub and Brekken, 2020). Our studies suggest that PtS may additionally function as an immune checkpoint via its capacity to promote the induction of immunosuppressive CD138^{hi} plasmablast responses. To directly test the relevance of PtS exposure in promoting CD138^{hi} plasmablast responses during experimental malaria, we employed both biological and genetic approaches to manipulate

PtS exposure and PtS receptor signaling. Consistent with our ex vivo B cell differentiation data, administration of mch1N11 to *Plasmodium*-infected mice reduced the absolute number of CD138^{hi} plasmablasts (Fig. 4 A) and increased the total numbers of GC B cells (Fig. 4 B) and GC–T follicular helper (Tfh) cells (Fig. 4 C) by 20–40%. Notably, mch1N11-mediated abrogation of CD138^{hi} plasmablast accumulation and augmented GC reactions were further associated with elevated class-switched, parasite-specific serum IgG antibody responses (Fig. 4 D) and enhanced parasite control (Fig. 4 E), which is in line with our recent report establishing the immunosuppressive function of CD138^{hi} plasmablasts during *Plasmodium* infection (Vijay et al., 2020).

PtS can either directly or indirectly engage a number of receptors to mediate its functions, including Tim1 and Axl. To distinguish between direct and indirect PtS signaling and begin to interrogate the biological relevance of specific PtS receptors, we generated mixed bone marrow chimeric mice containing either WT and *Tim1*^{-/-} or WT and *Axl*^{-/-} compartments at 1:1 ratios, which allowed us to dissect the role of B cell-intrinsic PtS signaling in the same infected host. While plasmablast differentiation was equivalent among both *Tim1*^{-/-} and WT compartments (Fig. 4 F), we observed greater than fivefold reductions in plasmablast differentiation among *Axl*^{-/-} B cells compared with WT B cells in the same *Plasmodium*-infected host (Fig. 4 G). Together, the composite of our ex vivo and in vivo biochemical, transcriptomic, and genetic studies supports the hypothesis that either RBC damage or destruction may expose PtS that can signal via Axl and function together with polyclonal B activators, inflammatory cytokines, and PRR signaling cascades to program the appearance and accumulation of immunosuppressive CD138^{hi} plasmablast populations.

Plasmablasts numerically dominate the initial B cell response during both *Trypanosoma* and *Plasmodium* blood-stage infections, and prominent features of both human and experimental malaria and trypanosomiasis include polyclonal B cell activation and the induction of nonparasite-specific antibody responses and hyperglobulinemia (Freeman and Parish, 1978; Rosenberg, 1978; Wenisch et al., 1996). Our recent studies identified the immunosuppressive mechanisms and consequences of these massive plasmablast expansions (Vijay et al., 2020), and our current experiments support the model that IFN- γ and PRR signaling in combination with hemolysis-associated PtS exposure promote the differentiation of these immunosuppressive B cells. Our data further support that during pathological insults characterized by inflammation and hemolysis, PtS blockade has the potential to boost the immune function and protective immunity.

Our findings are particularly timely given multiple reports describing poor clinical outcomes associated with high-magnitude plasmablast responses (Thevarajan et al., 2020; Woodruff et al., 2020 Preprint) and reduced GC responses

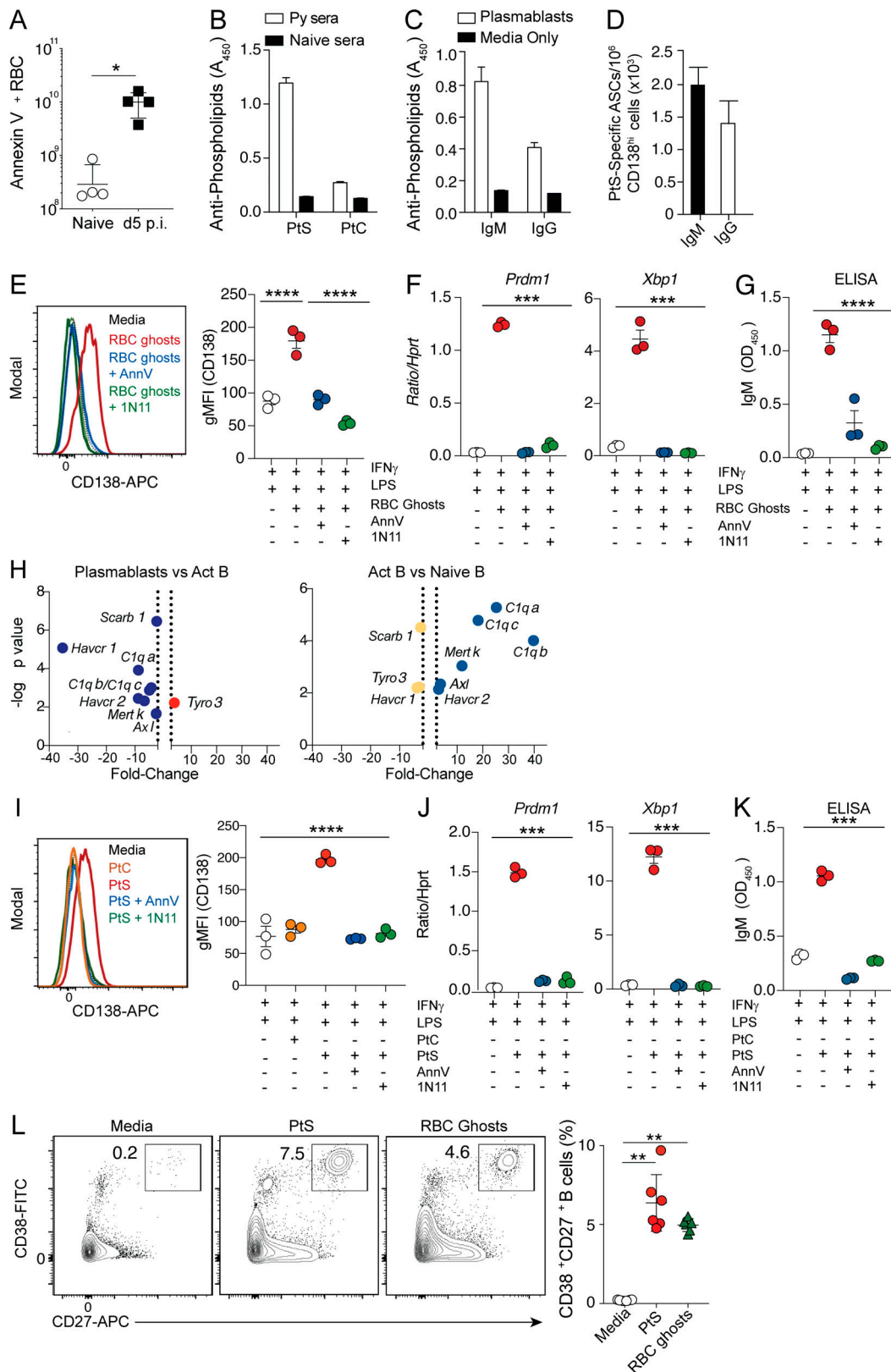


Figure 3. **PtS promotes plasmablast formation.** (A) Summary graph showing the number of Annexin V-positive RBCs/ml of blood in naive and *Py*-infected mice as a measure of PtS exposure. *n* = 4 mice/group; mean ± SD, representative of two biologically independent experiments. (B) Detection of PtS- and PtC-specific IgM antibodies in sera (1:100 dilution) of day 10 *Py*-infected mice or naive WT mice. *n* = 10 mice; mean ± SEM, pooled from four independent experiments. (C and D) Sort-purified CD138^{hi}IgD^{neg} plasmablasts from day 10 *Py*-infected mice were cultured for 20 h, and parasite lysate-specific IgM- and IgG-secreting antibody-secreting cells were detected by ELISA (C) or ELISPOT (D). *n* = 6 mice; mean ± SEM, pooled from two independent experiments.

(E–G) B cells from naive mice were cultured ex vivo for 3 d in media containing IFN- γ and LPS in the presence or absence of RBC ghosts or RBC ghosts plus Annexin V (AnnV) or RBC ghosts plus mch1N11. Representative histograms and summary data showing geometric mean fluorescence intensity (gMFI) of CD138 expression (E), summary data comparing mRNA expression of *Prdm1* and *Xbp1* relative to *Hprt* (F), and IgM antibody titers in the supernatant as detected by ELISA (G). $n = 3$ mice/group, mean \pm SEM. Each data point reflects the mean of two technical replicates; data are representative of four biologically independent experiments. (H) Volcano plot showing relative expression of receptors capable of binding to PtS when comparing either plasmablasts and activated B (Act B) cells (left) or activated B cells and naive B cells (right). Dotted vertical lines demarcate positive versus negative log₂(fold change). (I–K) B cells from naive mice were cultured ex vivo for 3 d in media containing IFN- γ and LPS in the presence or absence of PtC or PtS liposomes or PtS liposomes plus AnnV or PtS liposomes plus mch1N11. Representative histograms and summary data showing gMFI of CD138 expression (I), summary data comparing mRNA expression of *Prdm1* and *Xbp1* relative to *Hprt* (J), and IgM antibody titers in the supernatant as detected by ELISA (K). $n = 3$ mice/group, mean \pm SEM. Each data point reflects the mean of two technical replicates; data are representative of four biologically independent experiments. (L) Representative plots showing the differentiation of CD38⁺CD27⁺ human plasma cells from naive peripheral B cells cultured ex vivo in the presence of PtS liposomes or autologous RBC ghosts. $n = 2$ human leukocyte reduction system (LRS) blood cones with three wells/treatment group; mean \pm SEM, data are representative of two biologically independent experiments. Significance was calculated using one-way ANOVA (E–G and I–K) and Mann-Whitney test (A and L). *, $P < 0.05$; **, $P < 0.01$; ***, $P < 0.001$; ****, $P < 0.0001$.

(Kaneko et al., 2020; Mathew et al., 2020) in COVID-19 patients. The appearance of SARS-CoV-2-induced plasmablast responses was correlated not only to systemic inflammation, suggesting that other B cell activation stimuli, possibly PtS, may contribute to their differentiation and expansion. Indeed, hemolytic anemia has also been well documented during various stages of COVID-19 disease (Hindilerden et al., 2020a; Hindilerden et al., 2020b; Lazarian et al., 2020). It will be of interest to determine whether

the mechanisms governing plasmablast formation following SARS-CoV-2 infection is driven by hemolysis as well as determine whether plasmablasts exert either protective functions or immunosuppressive functions during COVID-19.

Our finding that polyclonal B cell activation signals, such as inflammatory cytokine signaling and/or TLR and PRR activation cascades, act in concert with PtS receptor signaling to promote optimal CD138^{hi} plasmablast differentiation is also consistent

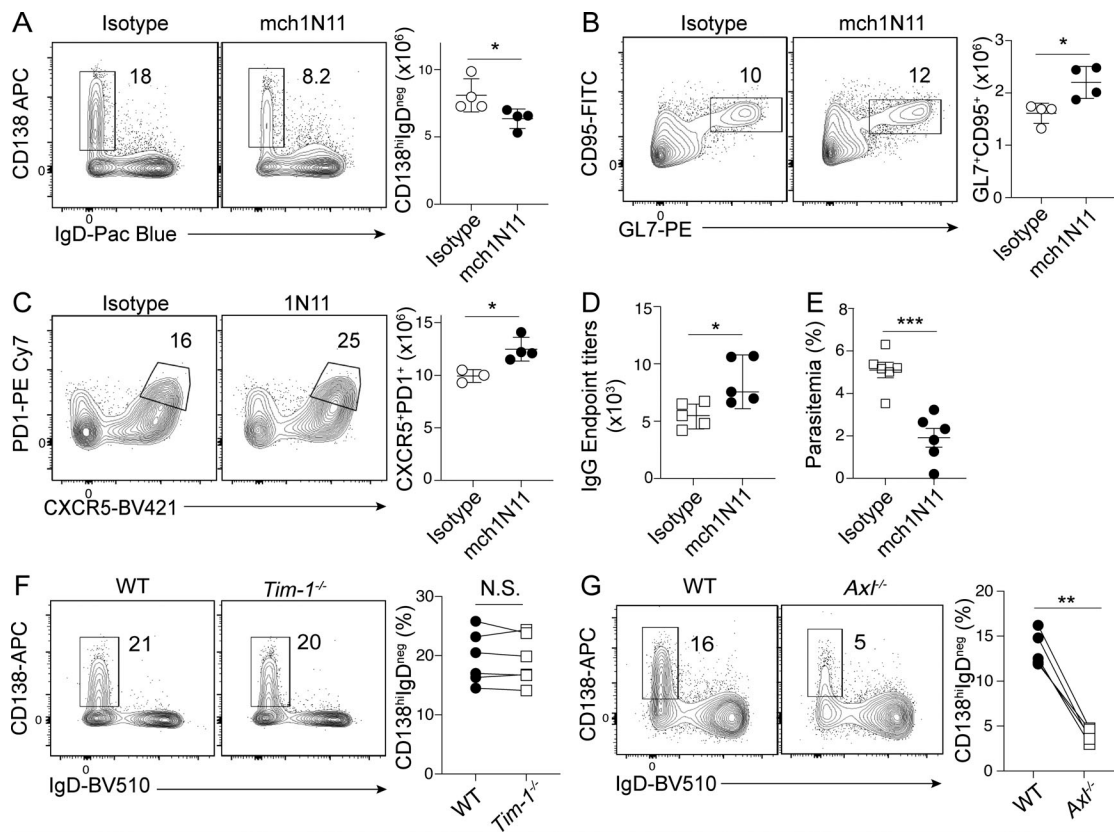


Figure 4. **PtS blockade inhibits plasmablast responses and improves humoral immunity.** (A–E) C57BL/6 mice were infected with *Py* and treated with mch1N11 or isotype control from days 5 to 7 p.i. Representative plots and summary graphs showing splenic plasmablasts (CD138^{hi}IgD^{neg}) on day 10 p.i. (A), CD95⁺GL7⁺ B (GC) cells (B), and CXCR5⁺PD1⁺ CD4 (GC-Tfh) cells on day 21 p.i. (C). $n = 4$ mice/group; mean \pm SD, representative of two biologically independent experiments. (D) Summary graphs showing parasite-specific serum IgG antibody end point titers on day 21 p.i. $n = 5$ mice/group; mean \pm SD, representative of two biologically independent experiments. (E) Summary graph showing frequency of infected RBCs on day 10 p.i. $n = 6$ mice/group, mean \pm SD, pooled from two biologically independent experiments. (F and G) 50:50 bone marrow chimeras using *Tim1*^{-/-} and WT cells (F) or *Axl*^{-/-} and WT cells (G) were generated and infected with 1×10^6 *Py* pRBCs. Representative plots and summary graphs showing frequency of splenic plasmablasts (CD138^{hi}IgD^{neg}) derived from each genotype on day 10 p.i. are shown. Connecting lines match gene knockout and WT B cells within each individual chimeric mouse. Significance was calculated using Mann-Whitney test (A–E) and paired *t* test (F and G). *, $P < 0.05$; **, $P < 0.01$; ***, $P < 0.001$.

with reports showing that PtS-mediated modulation of leukocyte biology requires multiple inputs (Bosurgi et al., 2017; Chen et al., 2012). Our transcriptomic analyses show that compared with CD138^{hi} plasmablasts, both resting and activated B cells expressed higher levels of several PtS receptors and that these expression patterns are consistent with the model that CD138^{hi} plasmablasts are terminally differentiated cells that likely no longer respond to PtS-associated signaling; the analyses also show that PtS acts on precursor populations, including other activated B cell subsets and potentially naive B cells, to potentiate their differentiation into plasmablasts.

To identify the specific PtS receptors that contribute to plasmablast differentiation, we focused on Tim1, which is reported to shape B cell differentiation (Ma et al., 2011), and Axl, which may be induced under conditions prevalent during *Plasmodium* infection. Indeed, hypoxia, which is a key feature of blood-stage *Plasmodium* infection (unpublished data) has been shown to stabilize and enhance Axl signaling (Mishra et al., 2012). Moreover, Axl signaling via PtS requires GAS6, which binds PtS via its “Gla” domain to activate the PI3K/AKT pathway and transduce intracellular signals that promote cell proliferation (Ruan and Kazlauskas, 2012), and PI3K signaling is essential for the differentiation of plasmablasts (Omori et al., 2006). While these reports are consistent with our finding that B cell-intrinsic Axl expression is critical for optimal plasmablast differentiation, our data do not rule out the potential contributions of other PtS receptors that share intracellular signaling cascades, such as Tyro3 (Stitt et al., 1995). Notably, multiple drugs targeting Axl have entered clinical trial, which raises the possibility that the PtS–GAS6–Axl pathway might serve as a therapeutic target to improve patient outcomes during malaria or other inflammatory pathologies associated with anemia and hemolysis and the exuberant expansion of plasmablasts.

In summary, we find that the preferential induction and differentiation of plasmablasts was associated with polyclonal B cell activation stimuli that include IFN- γ and PRR signaling and PtS exposure. Targeting these pathways significantly reduced plasmablast expansions, and blocking PtS exposure in vivo improved host resistance to *Plasmodium* infection. Collectively, our data support that immunotherapeutic strategies that include combinatorial targeting of multiple immune checkpoint pathways, including PtS, may prove effective for promoting resistance to a variety of infections.

Materials and methods

Animals, infections, and parasitemia quantification

The University of Iowa institutional animal care and use committee approved all experiments. C57BL/6 WT (JAX stock 002288), *Ifngr1*^{-/-} (JAX stock 025545), and MD4 (JAX stock 002595) mice were purchased from The Jackson Laboratory. C57BL/6 *Myd88*^{-/-} and *Ticam1*^{-/-} were generous gifts from Michelle Callegan (University of Oklahoma Health Sciences Center, Oklahoma City, OK); *Tim1*^{-/-} mice were a gift from Paul Rothman (Johns Hopkins, Baltimore, MD); and *Axl*^{-/-} bone marrow was a generous gift from Carla Rothlin (Yale University, New Haven, CT). Infections in experimental mice were initiated by either

serial transfer (i.v.) of 10⁶ *Plasmodium yoelii* (*Py*; American Type Culture Collection) parasitized RBCs (pRBCs) derived from a single donor C57BL/6 mouse, or i.p. injections of either 2.5 × 10⁶ PFUs of LCMV-Arm or 5,000 *Tb* Antat1.1 parasites (*Tb*; a generous gift from Kent Hill, University of California, Los Angeles, Los Angeles, CA). In some experiments, *Py*-infected mice were treated with 500 μ g of either α -IFN- γ (clone XMG1.2; BioXcell) or rat IgG1 isotype control or with 400 μ g of either mouse chimeric PtS-blocking antibody clone mch1N11 or mouse IgG2a (clone 1.18.4; BioXcell) isotype control, as indicated in the figure legends. Parasitemia was measured using flow cytometry as described (Malleret et al., 2011; Villarino et al., 2016).

ELISA and ELISpot

ELISA plates (Nunc) were coated overnight with either *Py* parasite lysate (18 μ g/ml; in-house), *Py* Hep17 (0.5 μ g/ml; Dr. Scott Lindner, Penn State University, State College, PA), HEL (0.5 μ g/ml; Sigma-Aldrich), ovalbumin (0.5 μ g/ml; Sigma-Aldrich), 4-Hydroxy-3-nitrophenylacetyl (26) conjugated to BSA (0.5 μ g/ml; Biosearch Technologies), LPS (*Escherichia coli* or *Salmonella enterica* serovar Minnesota; 1 μ g/ml; Sigma-Aldrich), flagellin from *S. enterica* serovar Typhimurium (1 μ g/ml; Dr. Matam Vijay-Kumar, Penn State University, State College, PA), anthrax protective antigen (recombinant from *Bacillus anthracis*; 0.5 μ g/ml; List Biological Laboratories, Inc.), and DNA, MB grade, from fish sperm (1 μ g/ml; Roche). For lipid ELISA, plates were coated with PtC or PtS (Avanti Polar Lipids; 40 μ g/ml each in chloroform). For IgM ELISA from naive B cell cultures, Nunc plates were coated with goat anti-mouse IgM antibody (1 μ g/ml) overnight. Plates were blocked with 2.5% BSA + 5% normal goat serum, and serum and culture supernatant samples were serially diluted and reacted for 24 h, and antigen- or *Py*-specific or IgM antibodies were detected with (1:500) HRP-conjugated goat anti-mouse IgM or IgG. The SureBlue reserve TMB Kit (KBL) was used as a substrate, and absorbance was assessed with a Spectra Max 340 (Molecular Devices). End point titers were extrapolated from sigmoidal 4PL (where X is log concentration) standard curve for each sample. The threshold for end point titers is the mean plus 2 \times SD of signal detected using sera from naive mice. For ELISpot, clear polypropylene plates (Nunc) were coated with PtS (50 μ g/ml) in chloroform (Avanti Polar Lipids). Plates were washed with PBS and blocked for at least 2 h with PBS/2.5% BSA/5% goat serum. CD19⁺CD138^{hi}IgD^{lo} B cells were sort-purified from day 10 *Py*-infected mice. Serial dilutions of cells in supplemented IMDM were added to each well for 20 h at 37°C with 5% CO₂. Following extensive washes with PBS/0.05% Tween 20, HRP-conjugated goat anti-mouse IgM and IgG was added overnight at 4°C. Spots were developed with 3-amino-9-ethylcarbazole.

Bone marrow chimeras

For B^{WT} and B^{Ifn γ rr1^{-/-}} chimeras, WT recipient (CD45.1) mice were irradiated with 475 rads twice separated by 4 h and bone marrow from either WT (CD45.2) or IFN γ R^{-/-} (CD45.2); μ MT (immunoglobulin heavy chain mu-deficient; *Ighm*^{-/-}) donors were mixed in 1:9 ratios, and 10⁷ cells were injected i.v. into the recipients. For WT:*Axl*^{-/-} (50:50) chimeras, CD45.1 recipient

mice were irradiated with 475 rads twice separated by 4 h, bone marrow from WT (CD45.1) and *Axl*^{-/-} (CD45.2) was mixed 1:1, and 10⁷ cells were injected i.v. into recipients. For WT:*Timl*^{-/-} (50:50) chimeras, *Rag1*^{-/-} recipient mice were irradiated once with 475 rads, bone marrow from WT (CD45.1) and *Timl*^{-/-} (CD45.2) was mixed 1:1, and 10⁷ cells were injected i.v. into recipients. All mice were maintained on Uniprim diet (Envigo) for 2–3 wk. Chimerism was assessed at 6 wk, and mice were infected with *Py* at 8 wk.

Bulk RNA sequencing and GSEA analyses

The three different B cell populations (resting B cells, activated B cells, and plasmablasts) were flow-sorted from four *Py*-infected mice on day 10 p.i., and RNA was extracted using the NucleoSpin RNA kit (Takara Bio USA Inc.) following the manufacturer's protocol. RNA integrity and quantity were determined using Tape Station Bioanalyzer (Agilent), with all samples showing RNA integrity numbers >8. Illumina library creation protocol was used to create a strand-specific RNA sequencing library. After pooling, the indexed libraries were sequenced using an Illumina NextSeq 550 sequencer using paired-end chemistry with 50-bp read length. FastQC (<http://www.bioinformatics.babraham.ac.uk/projects/fastqc/>) was used to assess the quality of sequence reads, which were aligned using STAR aligner (Dobin et al., 2013) to the mouse genome version mm10. Gene expression profiles were computed using featureCounts (Liao et al., 2014). Differentially expressed genes were identified using Partek GS software, and genes with significant changes (adjusted P value <0.05 and fold change >2 or less than -2) were filtered. Differentially expressed gene lists were generated using Partek GS software, and Ingenuity Pathway Analysis software (Qiagen Bioinformatics) was used to identify the underlying molecular pathways involving the differentially expressed genes. Sequences are deposited in the Gene Expression Omnibus under accession no. GSE134548.

Single-cell RNA sequencing and repertoire analyses

Naive B cells (CD19⁺CD138^{lo}IgD⁺) and plasmablasts (CD19⁺CD138⁺IgD^{neg}) from day 10 *Py*-infected mice (*n* = 3) were sort-purified (BD FACSAria II). Cells were partitioned into nanoliter-scale Gel Bead-In-EMulsions to achieve single-cell resolution for a maximum of 10,000 individual cells per sample. Using the Chromium Single Cell 5' Library and Gel Bead Kit (1000006; 10x Genomics), poly-adenylated mRNA from an individual cell was tagged with a unique 16-bp 10× barcode and 10-bp Unique Molecular Identifier. Full-length cDNA was generated, and V(D)J target enrichment was performed using the Chromium Single Cell V(D)J Enrichment Kit, Mouse B Cell (PN-1000072; 10x Genomics). The cDNA amplicon size for the library (~700 bp) was optimized using enzymatic fragmentation and size selection, and the concentration of the 10x single-cell library was determined through the Agilent High Sensitivity DNA Kit (Agilent). The single-cell V(D)J target enrichment libraries were sequenced on the Illumina HiSeq-4000 sequencer (The NUSeq Core facility; Northwestern University) at 150 × 150 bp paired end to target >5,000 reads per cell. We adopted Cell Ranger 3.0.2 (<https://support.10xgenomics.com/single-cell->

[gene-expression/software/pipelines/latest/what-is-cell-ranger](https://support.10xgenomics.com/single-cell-gene-expression/software/pipelines/latest/what-is-cell-ranger)) for raw sequencing process. All raw short reads were assembled by Cell Ranger, and then the assembled reads were mapped to the mm10 mouse genome using cellranger v1.3.1. V(D)J genes were exported into FASTA files. VH gene usage by naive B cells and plasmablasts was visualized using the “ggplot2” and “treemapify” packages, and the Shannon Index for each dataset was determined using the “vegan” package in R. For comparison of v gene locus usage of naive B cell and plasmablast populations, we calculated log₂ fold changes and statistical significance, via χ^2 tests, based on percentage of each v locus used by each population. In the volcano plot, the P value cutoff was equal to or less than 0.05, and the cutoff of log₂(fold change) was 1. All up-regulated and down-regulated v gene loci are labeled on the plot. Sequences are deposited in the Gene Expression Omnibus under accession no. GSE154910.

Quantitative real-time PCR

The three different B cell populations (resting B cells, activated B cells, and plasmablasts) were flow-sorted from four *Py*-infected mice on day 10 p.i., and RNA was extracted as described above. 2 µg of RNA was used for cDNA synthesis. 1 µl cDNA was added to 19 µl of PCR mixture containing 2X PowerUp SYBR Green Master Mix and 0.2 µM of forward or reverse primers. Amplification was performed in a QuantStudio3 thermocycler (Applied Biosystems). Primer sequences are as follows: house-keeping gene hypoxanthine phosphoribosyltransferase (*Hprt*), (forward) 5'-ACCCAGTGCTGGAGAAATTG-3' and (reverse) 5'-CTCGAGCAAGTCTTTCAGTCC-3'; *Prdm-1*, (forward) 5'-TAGACTTCACCGATGAGGGG-3' and (reverse) 5'-GTATGCTGCCAACAA CAGCA-3'; and *Xbp-1*, (forward) 5'-CCTGAGCCCGGAGGAGAA-3' and (reverse) 5'-CTCGAGCAGTCTGCGCTG-3'. Cycle threshold (Ct) values were normalized to those of *Hprt* by the following equation: $\Delta Ct = Ct_{(\text{gene of interest})} - Ct_{(\text{HPRT})}$. All results are shown as a ratio of HPRT calculated as $2^{-(\Delta Ct)}$.

PHZ preparation and treatment

PHZ was purchased from Sigma-Aldrich (114715). 1 mg of PHZ (as supplied) was suspended in 1 ml of sterile PBS to achieve a concentration of 0.67 mg/ml. LCMV-Arm-infected mice were treated with 186 µl of the solution i.p. on day 3 p.i.

PtS and PtC liposome preparation

1, 2-Diacyl-sn-glycero-3-phospho-L-serine (PtS; P7769) and L- α -PtC (P7443) were purchased from Sigma-Aldrich. 5 mg of lyophilized PtS or PtC (as supplied) was resuspended in 3.2 ml of sterile PBS to achieve 2-mM concentration and sonicated on ice for 15 min until the micelles were formed. The solution was stored at -20°C until used.

RBC ghosts preparation

WT C57BL/6 mice were exsanguinated using heparinized Nattelson blood collection tubes under anesthesia. RBC ghosts were prepared as previously described (Gupta et al., 2014). Briefly, blood was rinsed with twice the volume of osmotically balanced 0.15M salt solution. The tube was centrifuged at highest speed for 1 min at 4°C to pellet the RBCs. The top layer containing

plasma was removed, and the remaining pellet was resuspended in osmotically balanced 0.15M salt solution and centrifuged at highest speed for 1 min at 4°C. After removing the supernatant, the blood pellet was resuspended in sterile deionized water by vigorous agitation to lyse the RBCs. The suspension was centrifuged at maximum speed for 5 min at 4°C. The top layer containing hemoglobin was removed, and the pellet was resuspended in sterile PBS at 30×10^6 RBCs/ml.

Ex vivo murine B cell cultures

Naive splenic B cells were enriched from single-cell suspension using a mouse B cell Isolation kit (Cat #130-090-862; Miltenyi Biotec) according to the manufacturer's protocol. 10^5 cells were plated per well in a 96-well plate in triplicates/group and cultured in the presence of IFN- γ (50 ng/ml; Peprotech) and LPS (1 μ g/ml; Sigma-Aldrich) in IMDM10 (IMDM + 10% FBS) in the presence or absence of either PtS liposomes (10 μ M; Sigma-Aldrich) or 50 μ l RBC ghosts for 3 d at 37°C (5% CO₂ humidified incubator). Plates were spun down and stained with appropriate fluorochrome-conjugated antibodies (as described elsewhere), and data were acquired on a FACSVerse flow cytometer and analyzed as described elsewhere.

Ex vivo human B cell cultures

Leukocyte reduction cones containing human peripheral blood drawn from unidentified infection-naive volunteers were obtained from DeGowin blood center at University of Iowa. Blood was diluted 1:1 with PBS (Ca²⁺ Mg²⁺; HyClone) and carefully layered on top of Lymphocyte Separation Media (Corning) in 50-ml tubes, and lymphocytes were separated following the manufacturer's protocol. Untouched B cells were separated from the lymphocytes using Mojosort Human pan B cell isolation kit (Biolegend) according to the manufacturer's protocol. 10^5 naive human B cells in the presence of α -IgM (10 μ g/ml; Jackson Immunoresearch) and α -CD40 (1 μ g/ml; Biolegend) were cultured in IMDM10 (IMDM + 10% FBS) in the presence or absence of either PtS liposomes (10 μ M; Sigma-Aldrich) or RBC ghosts for 3 d at 37°C (5% CO₂ humidified incubator). Plates were spun down and stained with appropriate fluorochrome-conjugated antibodies, and data were acquired on a FACSVerse flow cytometer and analyzed as described below.

Cell staining and flow cytometry

For cellular analyses of splenic cells, mouse spleens were forced through a mesh to generate single-cell suspensions. The single-cell suspension of splenocytes was subjected to RBC lysis and was counted and suspended at 10^6 cells/100 μ l. Fc receptors were blocked using Fc block/CD16/32 (clone 2.4G2) in FACS buffer (PBS + 0.09% sodium azide + 2% FCS) for 15 min at 4°C followed by cell-specific staining protocols as described below. For detecting GC-Tfh-like cells, cells were stained with purified rat α mouse CXCR5 (1:100; clone 2G8; BD Biosciences) in Tfh staining buffer (PBS + 0.09% sodium azide + 2% FCS + 0.5% BSA + 2% mouse serum) for 1 h at 4°C. Cell were washed in FACS buffer, spun at 300 \times g for 5 min at 4°C, and suspended in Biotin SP-conjugated Affinipure Goat-anti-rat IgG (H+L) F(ab) (1:1,000; Jackson Immunoresearch) in Tfh staining buffer and

incubated for 30 min at 4°C. Cells were washed in FACS buffer, spun at 300 \times g for 5 min at 4°C, and suspended in an antibody cocktail containing CD4-PerCP Cy5.5 (1:300; clone GK1.5; BioLegend), CD44-AF700 (1:1,000; clone IM7; BioLegend), CD11a-FITC (1:300; clone M17/4; BD Biosciences), PD-1-PE or PE-Cy7 (1:300; clone RMP1-14; BioLegend), and streptavidin-BV421 (1:500) and incubated 30 min at 4°C. The cells were washed with FACS buffer as before and suspended in FACS buffer before acquisition. For B cell staining, cells were stained with B220-PerCP-Cy5.5 (1:300; clone RA3-6B2; BioLegend), CD19-AF700 or PE (1:300; clone 6D5; BioLegend), IgD-Pac Blue or BV510 (1:500; clone 11-26c.2a; BioLegend), CD138-APC or Pac Blue (1:250; clone 281-1; BioLegend; for plasmablast staining); GL7-PE (1:300; BioLegend), and CD95-FITC (1:300; clone Jo2; BD Biosciences; for GC B cell staining). For phospho-Syk (pSyk) staining, B cells were surface stained and permeabilized using the Transcription factor staining kit (Tonbo) and incubated with anti-mouse/human pSyk antibody (0.06 μ g/ 10^6 cells; clone mochlct; Invitrogen) or mouse IgG1 κ isotype (0.06 μ g/ 10^6 cells; clone P3.6.2.8.1; Invitrogen) according to the manufacturer's protocol. For Annexin V staining, Annexin V staining buffer kit (Cat #422201) was used according to the manufacturer's protocol. For human B cell staining, 200 μ l of blood was stained with surface antibodies to CD19 (FITC; clone HIB19), CD27 (AF700; clone M-T271), and CD38 (BV785; clone HIT2).

Statistical analysis

Statistical analyses, end point titers, and overall parasite burden, represented as area under the curve for rodent studies, were performed using GraphPad Prism 6 software (GraphPad). Specific tests of statistical significance are detailed in the figure legends. To calculate statistical differences in Fig. 1 G, we performed 1,000 independent runs of Jack knife resampling on plasmablast populations (randomly picked $n = 225$ samples from plasmablast population) and then performed χ^2 test for each round between the naive B cell population and resampled the plasmablast population.

Data availability

All data are available from the corresponding author upon request.

Online supplemental material

Fig. S1 shows the cytometry gating strategy, pSyk phosphoflow, serum ELISA data, statistical analyses of single-cell RNA data, and a volcano plot of VH loci expression among plasmablasts and naive B cells. Fig. S2 shows serum ELISA data from infected MD4 mice and plasmablast responses in *Leishmania*, influenza, and VSV-infected mice, as well as mice subjected to cecal ligation and puncture. Fig. S3 shows Annexin V staining of B cells recovered from naive and *Plasmodium*-infected mice. Table S1 shows differentially enriched genes in plasmablasts and activated B cells.

Acknowledgments

We thank members of the Butler laboratory for helpful discussions, Drs. Ali Jabbari (University of Iowa) and Martin Richer

(McGill University) for critical review, and members of the University of Iowa Flow Cytometry Facility for cell sorting.

Research reported in this publication was supported by the National Cancer Institute (grant no. P30CA086862) and by the National Center for Research Resources of the National Institutes of Health (grant no. S10OD016199). This research was also supported by the National Institutes of Health/National Heart, Lung, and Blood Institute (T32HL007605 in support of J.J. Guthmiller) and the National Institutes of Health/National Institute of Allergy and Infectious Diseases (T32AI007511 in support of J.T. Johnson; R01AI134733 and R21AI139902 to W. Maury; P01AI097092 and HHSN272201400005C to P.C. Wilson; and R01AI125446 and R01AI127481 to N.S. Butler), and the US Department of Veterans Affairs (I01BX001983 and 2I01BX000536 to M.E. Wilson).

Author contributions: R. Vijay, J.J. Guthmiller, and A.J. Sturtz conceived, designed, and performed experiments and analyzed data. S. Crooks, J.T. Johnson, R.L. Pope, Y. Chen, K.J. Rogers, and N. Dutta performed experiments and provided technical assistance. R. Vijay, J.J. Guthmiller, L. Li, and L. Yu-Ling Lan contributed to bioinformatic analyses. J.E. Toombs, M.E. Wilson, P.C. Wilson, W. Maury, and R.A. Brekken provided critical reagents and technical assistance. R. Vijay and J.J. Guthmiller made the figures. R. Vijay wrote the manuscript. W. Maury, P.C. Wilson, R.A. Brekken, and N.S. Butler reviewed and edited the manuscript and figures. N.S. Butler supervised the studies.

Disclosures: R.A. Brekken reported grants from OncXerna Therapeutics outside the submitted work and had a patent to PS-targeting antibodies licensed (OncXerna Therapeutics). No other disclosures were reported.

Submitted: 5 November 2020

Revised: 10 February 2021

Accepted: 11 March 2021

References

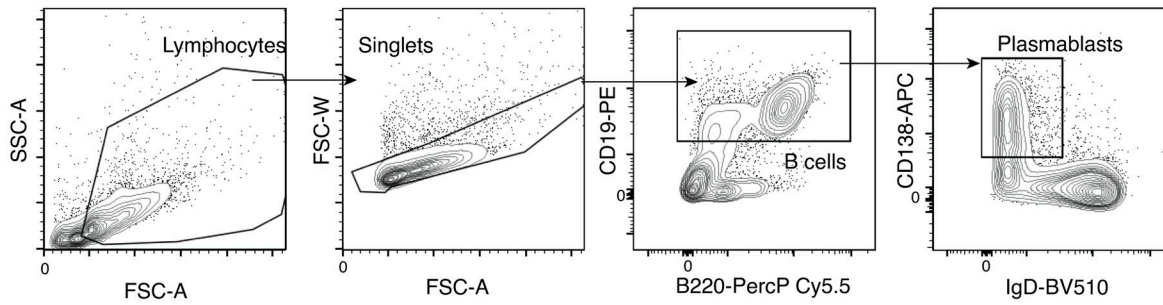
- Adams, S., H. Brown, and G. Turner. 2002. Breaking down the blood-brain barrier: signaling a path to cerebral malaria? *Trends Parasitol.* 18: 360–366. [https://doi.org/10.1016/S1471-4922\(02\)02353-X](https://doi.org/10.1016/S1471-4922(02)02353-X)
- Bosurgi, L., Y.G. Cao, M. Cabeza-Cabrero, A. Tucci, L.D. Hughes, Y. Kong, J.S. Weinstein, P. Licona-Limon, E.T. Schmid, F. Pelorosso, et al. 2017. Macrophage function in tissue repair and remodeling requires IL-4 or IL-13 with apoptotic cells. *Science.* 356:1072–1076. <https://doi.org/10.1126/science.aai8132>
- Chen, F., Z. Liu, W. Wu, C. Roza, S. Bowdridge, A. Millman, N. Van Rooijen, J.F. Urban Jr., T.A. Wynn, and W.C. Gause. 2012. An essential role for TH2-type responses in limiting acute tissue damage during experimental helminth infection. *Nat. Med.* 18:260–266. <https://doi.org/10.1038/nm.2628>
- Dayoub, A.S., and R.A. Brekken. 2020. TIMs, TAMs, and PS- antibody targeting: implications for cancer immunotherapy. *Cell Commun. Signal.* 18: 29. <https://doi.org/10.1186/s12964-020-0521-5>
- De Souza, J.B., K.H. Williamson, T. Otani, and J.H. Playfair. 1997. Early gamma interferon responses in lethal and nonlethal murine blood-stage malaria. *Infect. Immun.* 65:1593–1598. <https://doi.org/10.1128/IAI.65.5.1593-1598.1997>
- Dobin, A., C.A. Davis, F. Schlesinger, J. Drenkow, C. Zaleski, S. Jha, P. Batut, M. Chaisson, and T.R. Gingeras. 2013. STAR: ultrafast universal RNA-seq aligner. *Bioinformatics.* 29:15–21. <https://doi.org/10.1093/bioinformatics/bts635>
- Donati, D., L.P. Zhang, A. Chêne, Q. Chen, K. Flick, M. Nyström, M. Wahlgren, and M.T. Bejarano. 2004. Identification of a polyclonal B-cell activator

- in *Plasmodium falciparum*. *Infect. Immun.* 72:5412–5418. <https://doi.org/10.1128/IAI.72.9.5412-5418.2004>
- Donati, D., B. Mok, A. Chêne, H. Xu, M. Thangarajh, R. Glas, Q. Chen, M. Wahlgren, and M.T. Bejarano. 2006. Increased B cell survival and preferential activation of the memory compartment by a malaria polyclonal B cell activator. *J. Immunol.* 177:3035–3044. <https://doi.org/10.4049/jimmunol.177.5.3035>
- Fernandez-Arias, C., J. Rivera-Correa, J. Gallego-Delgado, R. Rudlaff, C. Fernandez, C. Roussel, A. Götz, S. Gonzalez, A. Mohanty, S. Mohanty, et al. 2016. Anti-Self Phosphatidylserine Antibodies Recognize Uninfected Erythrocytes Promoting Malarial Anemia. *Cell Host Microbe.* 19: 194–203. <https://doi.org/10.1016/j.chom.2016.01.009>
- Freeman, R.R., and C.R. Parish. 1978. Polyclonal B-cell activation during rodent malarial infections. *Clin. Exp. Immunol.* 32:41–45.
- Gupta, N., B. Patel, and F. Ahsan. 2014. Nano-engineered erythrocyte ghosts as inhalational carriers for delivery of fasudil: preparation and characterization. *Pharm. Res.* 31:1553–1565. <https://doi.org/10.1007/s11095-013-1261-7>
- Hindilerden, F., I. Yonal-Hindilerden, E. Akar, and K. Kart-Yasar. 2020a. Covid-19 associated autoimmune thrombotic thrombocytopenic purpura: Report of a case. *Thromb. Res.* 195:136–138. <https://doi.org/10.1016/j.thromres.2020.07.005>
- Hindilerden, F., I. Yonal-Hindilerden, E. Akar, Z. Yesilbag, and K. Kart-Yasar. 2020b. Severe Autoimmune Hemolytic Anemia in COVID-19 Infection, Safely Treated with Steroids. *Mediterr. J. Hematol. Infect. Dis.* 12: e2020053. <https://doi.org/10.4084/mjhid.2020.053>
- Ikeda, B.O., M. Lule, and R.J. Terry. 1977. Anaemia in trypanosomiasis: mechanisms of erythrocyte destruction in mice infected with *Trypanosoma congolense* or *T. brucei*. *Acta Trop.* 34:53–60.
- Iwakoshi, N.N., A.H. Lee, and L.H. Glimcher. 2003a. The X-box binding protein-1 transcription factor is required for plasma cell differentiation and the unfolded protein response. *Immunol. Rev.* 194:29–38. <https://doi.org/10.1034/j.1600-065X.2003.00057.x>
- Iwakoshi, N.N., A.H. Lee, P. Vallabhajosyula, K.L. Otipoby, K. Rajewsky, and L.H. Glimcher. 2003b. Plasma cell differentiation and the unfolded protein response intersect at the transcription factor XBP-1. *Nat. Immunol.* 4:321–329. <https://doi.org/10.1038/ni907>
- Kaneko, N., H.H. Kuo, J. Boucau, J.R. Farmer, H. Allard-Chamard, V.S. Mahajan, A. Piechocka-Trocha, K. Lefteri, M. Osborn, J. Bals, et al. Massachusetts Consortium on Pathogen Readiness Specimen Working Group. 2020. Loss of Bcl-6-Expressing T Follicular Helper Cells and Germinal Centers in COVID-19. *Cell.* 183:143–157.e13: E13. <https://doi.org/10.1016/j.cell.2020.08.025>
- King, T., and T. Lamb. 2015. Interferon- γ : The Jekyll and Hyde of Malaria. *PLoS Pathog.* 11:e1005118. <https://doi.org/10.1371/journal.ppat.1005118>
- Lamikanra, A.A., D. Brown, A. Potocnik, C. Casals-Pascual, J. Langhorne, and D.J. Roberts. 2007. Malarial anemia: of mice and men. *Blood.* 110:18–28. <https://doi.org/10.1182/blood-2006-09-018069>
- Lazarian, G., A. Quinquenel, M. Bellal, J. Siavellis, C. Jacquy, D. Re, F. Merabet, A. Mekinian, T. Braun, G. Damaj, et al. 2020. Autoimmune haemolytic anaemia associated with COVID-19 infection. *Br. J. Haematol.* 190:29–31. <https://doi.org/10.1111/bjh.16794>
- Liao, Y., G.K. Smyth, and W. Shi. 2014. featureCounts: an efficient general purpose program for assigning sequence reads to genomic features. *Bioinformatics.* 30:923–930. <https://doi.org/10.1093/bioinformatics/btt656>
- Ly, A., and D.S. Hansen. 2019. Development of B Cell Memory in Malaria. *Front. Immunol.* 10:559. <https://doi.org/10.3389/fimmu.2019.00559>
- Ma, J., Y. Usui, K. Takeda, N. Harada, H. Yagita, K. Okumura, and H. Akiba. 2011. TIM-1 signaling in B cells regulates antibody production. *Biochem. Biophys. Res. Commun.* 406:223–228. <https://doi.org/10.1016/j.bbrc.2011.02.021>
- Malleret, B., C. Claser, A.S. Ong, R. Suwanarusk, K. Sriprawatt, S.W. Howland, B. Russell, F. Nosten, and L. Rénia. 2011. A rapid and robust tri-color flow cytometry assay for monitoring malaria parasite development. *Sci. Rep.* 1:118. <https://doi.org/10.1038/srep00118>
- Mathew, D., J.R. Giles, A.E. Baxter, D.A. Oldridge, A.R. Greenplate, J.E. Wu, C. Alanio, L. Kuri-Cervantes, M.B. Pampena, K. D'Andrea, et al. UPenn COVID Processing Unit. 2020. Deep immune profiling of COVID-19 patients reveals distinct immunotypes with therapeutic implications. *Science.* 369:eabc8511. <https://doi.org/10.1126/science.abc8511>
- Mishra, A., J. Wang, Y. Shiozawa, S. McGee, J. Kim, Y. Jung, J. Joseph, J.E. Berry, A. Havens, K.J. Pienta, and R.S. Taichman. 2012. Hypoxia stabilizes GAS6/Axl signaling in metastatic prostate cancer. *Mol. Cancer Res.* 10:703–712. <https://doi.org/10.1158/1541-7786.MCR-11-0569>

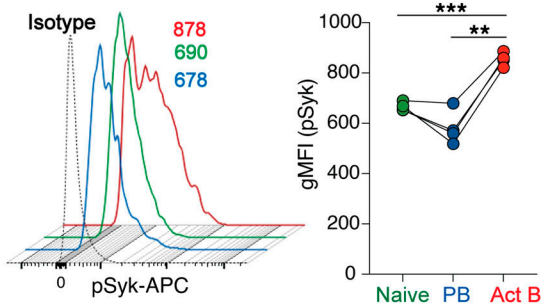
- Moxon, C.A., M.P. Gibbins, D. McGuinness, D.A. Milner Jr., and M. Marti. 2020. New Insights into Malaria Pathogenesis. *Annu. Rev. Pathol.* 15: 315–343. <https://doi.org/10.1146/annurev-pathmechdis-012419-032640>
- Omori, S.A., M.H. Cato, A. Anzelon-Mills, K.D. Puri, M. Shapiro-Shelef, K. Calame, and R.C. Rickert. 2006. Regulation of class-switch recombination and plasma cell differentiation by phosphatidylinositol 3-kinase signaling. *Immunity.* 25:545–557. <https://doi.org/10.1016/j.immuni.2006.08.015>
- Rivera-Correa, J., J.J. Guthmiller, R. Vijay, C. Fernandez-Arias, M.A. Pardo-Ruge, S. Gonzalez, N.S. Butler, and A. Rodriguez. 2017. Plasmodium DNA-mediated TLR9 activation of T-bet⁺ B cells contributes to auto-immune anaemia during malaria. *Nat. Commun.* 8:1282. <https://doi.org/10.1038/s41467-017-01476-6>
- Rivera-Correa, J., M.S. Mackroth, T. Jacobs, J. Schulze Zur Wiesch, T. Rolling, and A. Rodriguez. 2019. Atypical memory B-cells are associated with *Plasmodium falciparum* anemia through anti-phosphatidylserine antibodies. *eLife.* 8:e48309. <https://doi.org/10.7554/eLife.48309>
- Rosenberg, Y.J. 1978. Autoimmune and polyclonal B cell responses during murine malaria. *Nature.* 274:170–172. <https://doi.org/10.1038/274170a0>
- Ruan, G.X., and A. Kazlauskas. 2012. Axl is essential for VEGF-A-dependent activation of PI3K/Akt. *EMBO J.* 31:1692–1703. <https://doi.org/10.1038/emboj.2012.21>
- Scholzen, A., A.C. Teirlinck, E.M. Bijker, M. Roestenberg, C.C. Hermsen, S.L. Hoffman, and R.W. Sauerwein. 2014. BAFF and BAFF receptor levels correlate with B cell subset activation and redistribution in controlled human malaria infection. *J. Immunol.* 192:3719–3729. <https://doi.org/10.4049/jimmunol.1302960>
- Shaffer, A.L., M. Shapiro-Shelef, N.N. Iwakoshi, A.H. Lee, S.B. Qian, H. Zhao, X. Yu, L. Yang, B.K. Tan, A. Rosenwald, et al. 2004. XBPI, downstream of Blimp-1, expands the secretory apparatus and other organelles, and increases protein synthesis in plasma cell differentiation. *Immunity.* 21: 81–93. <https://doi.org/10.1016/j.immuni.2004.06.010>
- Simone, O., M.T. Bejarano, S.K. Pierce, S. Antonaci, M. Wahlgren, M. Troye-Blomberg, and D. Donati. 2011. TLRs innate immunoreceptors and Plasmodium falciparum erythrocyte membrane protein 1 (PfEMP1) CIDR1 α -driven human polyclonal B-cell activation. *Acta Trop.* 119: 144–150. <https://doi.org/10.1016/j.actatropica.2011.05.005>
- Stellrecht, K.A., and A.T. Vella. 1992. Evidence for polyclonal B cell activation as the mechanism for LCMV-induced autoimmune hemolytic anemia. *Immunol. Lett.* 31:273–277. [https://doi.org/10.1016/0165-2478\(92\)90126-9](https://doi.org/10.1016/0165-2478(92)90126-9)
- Stijlemans, B., P. De Baetselier, S. Magez, J.A. Van Ginderachter, and C. De Trez. 2018. African Trypanosomiasis-Associated Anemia: The Contribution of the Interplay between Parasites and the Mononuclear Phagocyte System. *Front. Immunol.* 9:218. <https://doi.org/10.3389/fimmu.2018.00218>
- Stitt, T.N., G. Conn, M. Gore, C. Lai, J. Bruno, C. Radziejewski, K. Mattsson, J. Fisher, D.R. Gies, P.F. Jones, et al. 1995. The anticoagulation factor protein S and its relative, Gas6, are ligands for the Tyro 3/Axl family of receptor tyrosine kinases. *Cell.* 80:661–670. [https://doi.org/10.1016/0092-8674\(95\)90520-0](https://doi.org/10.1016/0092-8674(95)90520-0)
- Thevarajan, I., T.H.O. Nguyen, M. Koutsakos, J. Druce, L. Caly, C.E. van de Sandt, X. Jia, S. Nicholson, M. Catton, B. Cowie, et al. 2020. Breadth of concomitant immune responses prior to patient recovery: a case report of non-severe COVID-19. *Nat. Med.* 26:453–455. <https://doi.org/10.1038/s41591-020-0819-2>
- Tran, T.M., S. Li, S. Doumbo, D. Doumbo, C.Y. Huang, S. Dia, A. Bathily, J. Sangala, Y. Kone, A. Traore, et al. 2013. An intensive longitudinal cohort study of Malian children and adults reveals no evidence of acquired immunity to *Plasmodium falciparum* infection. *Clin. Infect. Dis.* 57: 40–47. <https://doi.org/10.1093/cid/cit174>
- Vijay, R., J.J. Guthmiller, A.J. Sturtz, F.A. Surette, K.J. Rogers, R.R. Sompallae, F. Li, R.L. Pope, J.A. Chan, F. de Labastida Rivera, et al. 2020. Infection-induced plasmablasts are a nutrient sink that impairs humoral immunity to malaria. *Nat. Immunol.* 21:790–801. <https://doi.org/10.1038/s41590-020-0678-5>
- Villarino, N.F., G.R. LeCleir, J.E. Denny, S.P. Dearth, C.L. Harding, S.S. Sloan, J.L. Gribble, S.R. Campagna, S.W. Wilhelm, and N.W. Schmidt. 2016. Composition of the gut microbiota modulates the severity of malaria. *Proc. Natl. Acad. Sci. USA.* 113:2235–2240. <https://doi.org/10.1073/pnas.1504887113>
- von Herrath, M., B. Coon, D. Homann, T. Wolfe, and L.G. Guidotti. 1999. Thymic tolerance to only one viral protein reduces lymphocytic choriomeningitis virus-induced immunopathology and increases survival in perforin-deficient mice. *J. Virol.* 73:5918–5925. <https://doi.org/10.1128/JVI.73.7.5918-5925.1999>
- Wenisch, C., H. Wenisch, H.C. Bankl, M. Exner, W. Graninger, S. Loar-eesuwan, and H. Rumpold. 1996. Detection of anti-neutrophil cytoplasmic antibodies after acute *Plasmodium falciparum* malaria. *Clin. Diagn. Lab. Immunol.* 3:132–134. <https://doi.org/10.1128/CDLI.3.1.132-134.1996>
- White, N.J. 2018. Anaemia and malaria. *Malar. J.* 17:371. <https://doi.org/10.1186/s12936-018-2509-9>
- White, C., X. Yuan, P.J. Schmidt, E. Bresciani, T.K. Samuel, D. Campagna, C. Hall, K. Bishop, M.L. Calicchio, A. Lapierre, et al. 2013. HRG1 is essential for heme transport from the phagolysosome of macrophages during erythrophagocytosis. *Cell Metab.* 17:261–270. <https://doi.org/10.1016/j.cmet.2013.01.005>
- Woodruff, M., R. Ramonell, K. Cashman, D. Nguyen, A. Ley, S. Kyu, A. Saini, N. Haddad, W. Chen, J.C. Howell, et al. 2020. Critically ill SARS-CoV-2 patients display lupus-like hallmarks of extrafollicular B cell activation. *medRxiv.* <https://doi.org/10.1101/2020.04.29.20083717> (Preprint posted May 3, 2020) <https://doi.org/10.1101/2020.04.29.20083717>
- World Health Organization. 2020. World Malaria Report 2020. <https://www.who.int/publications/i/item/9789240015791> (accessed January 26, 2021).
- Wu, J., L. Tian, X. Yu, S. Pattaradilokrat, J. Li, M. Wang, W. Yu, Y. Qi, A.E. Zeituni, S.C. Nair, et al. 2014. Strain-specific innate immune signaling pathways determine malaria parasitemia dynamics and host mortality. *Proc. Natl. Acad. Sci. USA.* 111:E511–E520. <https://doi.org/10.1073/pnas.1316467111>
- Zhu, X., J. Liu, Y. Feng, W. Pang, Z. Qi, Y. Jiang, H. Shang, and Y. Cao. 2015. Phenylhydrazine administration accelerates the development of experimental cerebral malaria. *Exp. Parasitol.* 156:1–11. <https://doi.org/10.1016/j.exppara.2015.05.011>

Supplemental material

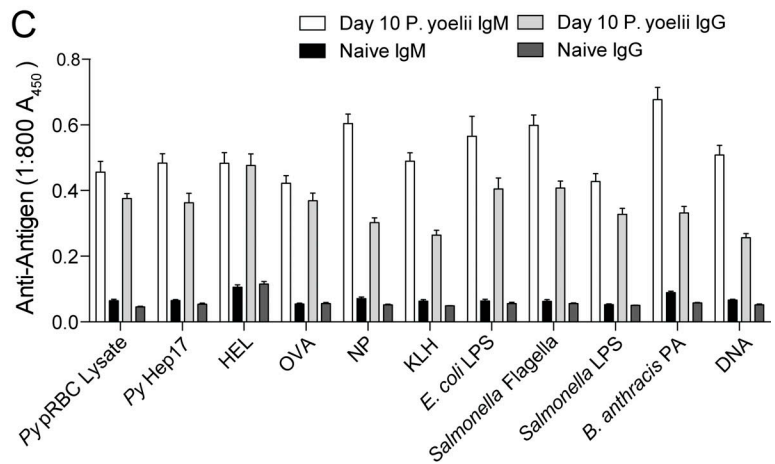
A Gating strategy for plasmablast determination



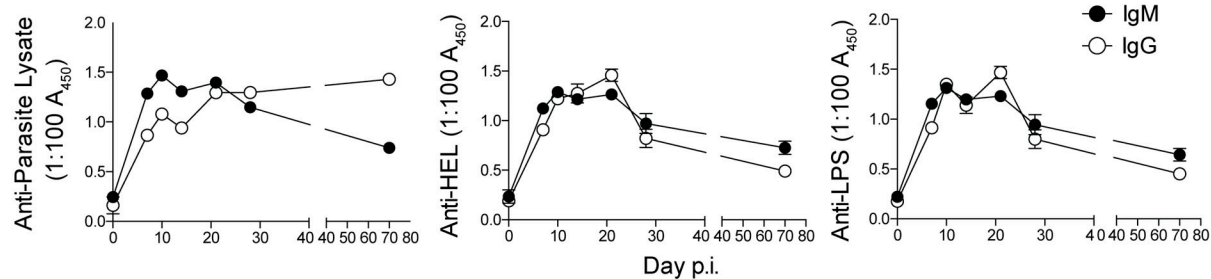
B



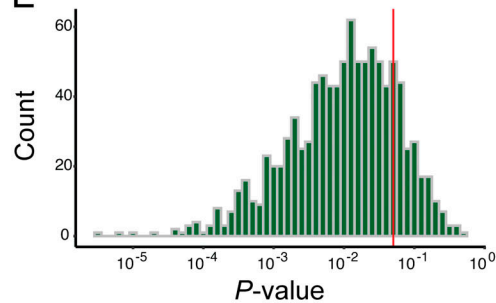
C



D



E



F

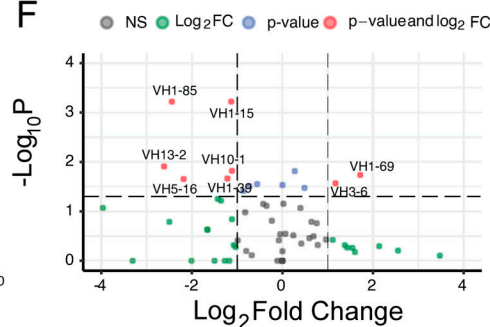


Figure S1. **Cytometry gating strategy, phosphoflow, serum ELISA data, and statistical analyses of single-cell RNA sequencing data.** (A) Gating strategy for identifying plasmablasts is shown. (B) *Py*-infected WT mice were harvested on day 6 p.i., and the B cell populations were evaluated for phosphorylation of Syk. Representative histograms and summary graphs showing geometric mean fluorescence intensity (gMFI) of pSyk on B cell subsets are shown. (C) Sera were collected from *Py*-infected WT mice on day 10 p.i., diluted 1:800, and reacted against the indicated parasite-, model-, microbial-, and self-specific antigens. $n = 20$ mice. Data are mean \pm SEM, pooled from five biologically independent experiments. (D) Longitudinal analyses of parasite lysate- (top), HEL- (bottom left), and LPS- (bottom right) specific serum IgM and IgG titers in *Py*-infected mice. $n = 6$ mice/time point; mean \pm SEM pooled from two biologically independent experiments, analyzed by Mann-Whitney. (E) Histogram of P value results of 1,000 Jack knife resampling χ^2 tests. (F) Volcano plot of VH loci expressed by plasmablast population relative to naive B cell repertoire. Act B, activated B; FC, fold change; FSC-A, forward scatter area; FSC-W, forward scatter width; NP, (4-hydroxy-3-nitrophenyl)acetyl antigen; PA, protective antigen; PB, plasmablast; PerCP, peridinin-chlorophyll-protein; scRNA, single-cell RNA; SSC-A, side scatter area.

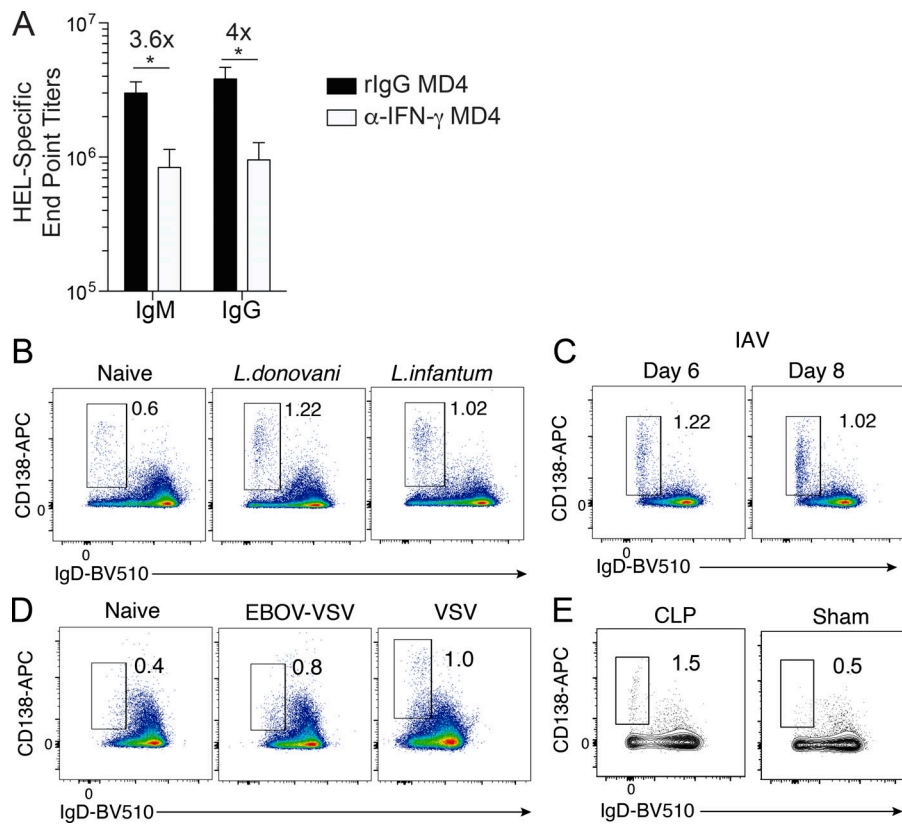


Figure S2. Serum ELISA data from infected MD4 mice and plasmablast responses in *Leishmania*, influenza, and VSV-infected mice, and mice subjected to cecal ligation and puncture. (A) MD4 mice were infected with 10^6 Py pRBCs and administered 500 μ g of α -IFN- γ ($n = 8$; clone XMGL2) or rIgG ($n = 6$) on days 0, 3, 6, and 9 p.i. HEL-specific IgM and IgG serum end point titers as measured by ELISA on day 10 p.i. Data are mean \pm SEM, representative of four independent experiments, analyzed using unpaired Mann-Whitney tests. (B–E) CD138^{hi}IgD^{neg} splenic plasmablast responses were evaluated on day 10 p.i. in WT mice infected i.v. with 2.5×10^7 of either *L. donovani* or *L. infantum* parasites ($n = 10$ mice/group; B) or intranasally with 100 IU of influenza A virus (IAV; $n = 5$; C); in IFNAR-deficient mice ($n = 6$) infected i.p. with 100 PFUs of recombinant VSV (EBOV-VSV; D, middle panel) or WT mice infected with high-dose (1×10^6 PFUs) VSV (D, right panel); or WT mice subjected to cecal ligation and puncture (CLP; $n = 4$) or sham surgery ($n = 4$; E). *, $P < 0.05$.

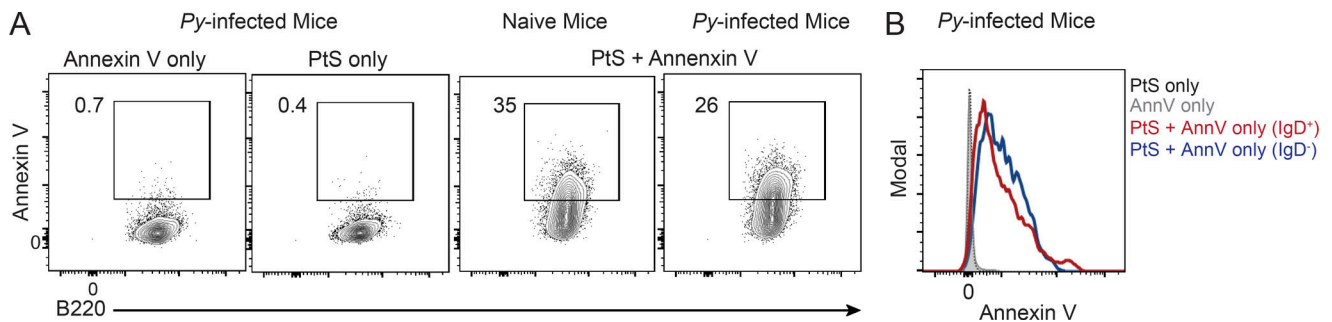


Figure S3. Annexin V staining of B cells recovered from naive and *Py*-infected mice. (A and B) Representative plots (A) and histograms showing geometric mean fluorescence intensity (B) of Annexin V (AnnV) staining, probing for PtS binding to B cells recovered from naive mouse (A, third panel) or on day 4 after *Py* infection (A, fourth panel, and B). $n = 3$ mice/group, representative of two biologically independent experiments.

Table S1 is provided online as an Excel file and shows differentially enriched genes in plasmablasts and activated B cells.